Instrument Science Report STIS 2018-02

A New Geometric-distortion Solution for STIS FUV-MAMA

S. Tony Sohn[1]

[1] Space Telescope Science Institute, Baltimore, MD

Monday 16th April, 2018

ABSTRACT

We derived a new geometric distortion solution for the STIS FUV-MAMA detector. To do this, positions of stars in 89 FUV-MAMA observations of NGC 6681 were compared to an astrometric standard catalog created using WFC3/UVIS imaging data to derive a fourth-order polynomial solution that transforms raw (x, y) positions to geometrically-corrected (x, y) positions. When compared to astrometric catalog positions, the FUV-MAMA position measurements based on the `IDCTAB` *showed residuals with an RMS of* ~ 30 *mas in each coordinate. Using the new* `IDCTAB`*, the RMS is reduced to* ~ 4 *mas, or 0.16 FUV-MAMA pixels, in each coordinate. The updated* `IDCTAB` *is now being used in the HST STIS pipeline to process all STIS FUV-MAMA images.*

Contents

Operated by the Association of Universities for Research in Astronomy, Inc., for the National Aeronautics and Space Administration.

1. Introduction

All detectors equipped on the HST suffer from geometric distortions due to the detectors not being exactly aligned with the focal plane. The degree of distortions varies significantly across different types of detectors, but it is important to correct the distortions for various applications such as measuring accurate positions for objects of interests, or combining images taken with different pointings/orientations.

For HST, ACS/WFC and WFC3/UVIS have been the main imaging devices since the *Servicing Mission 4* in 2009, and so both detectors have extremely well-calibrated distortion solutions (Kozhurina-Platais et al. 2009a, 2009b, 2015) that allow precision astrometry (e.g., Sohn et al. 2017). The STIS FUV-MAMA, on the other hand, have been lacking a good distortion solution. The first few attempts to calibrate the geometric distortion for STIS FUV-MAMA (Malumuth 1997; Walsh et al. 2001) lacked a sufficient amount of calibration data to create a reliable solution for the full detector. However, we now have a series of observations that allow us to derive the geometric distortion solution for the STIS FUV-MAMA. As part of the STIS MAMA full-field sensitivity monitor program, the globular cluster NGC 6681 has been routinely imaged by both the NUV- and FUV-MAMA every year since 1997 except for the period 2005–2009 when STIS was inoperable due to a failure of its Side-2 electronics. In addition, there are existing WFC3/UVIS images that cover the same field, so together, this provided us the opportunity to derive new geometric distortion solution for the STIS FUV-MAMA.

Our goal is to derive a geometric distortion solution for the STIS FUV-MAMA detector, and implement this as a reference file (`IDCTAB`) to be used in the HST pipeline. In this ISR, we describe the details of which data were used in the process, how we derived the solution, and what accuracies we have achieved. We also discuss the implementation of the derived geometric distortion solution.

2. Data

Deriving a geometric distortion solution for a given imaging device requires two sets of data. First is the standard astrometric catalog which provides the true positions of stars in a distortion-free frame. Second is the catalog of measured positions of stars in the observing mode of interest. Once these two catalogs are ready, distortion solution is derived by devising a mathematical solution that corrects the measured positions to the true ones. We have chosen to use stars in the globular cluster NGC 6681 to derive the distortion solution. This cluster was imaged in STIS FUV-MAMA, the detector we are deriving the solution for, and in WFC3/UVIS, a detector which already has a good geometric distortion solution (Kozhurina-Platais et al. 2009a, 2009b; Bellini et al. 2011). In Figure 1, we show the same NGC 6681 field imaged with the STIS FUV-MAMA (left) and WFC3/UVIS F336W (right).

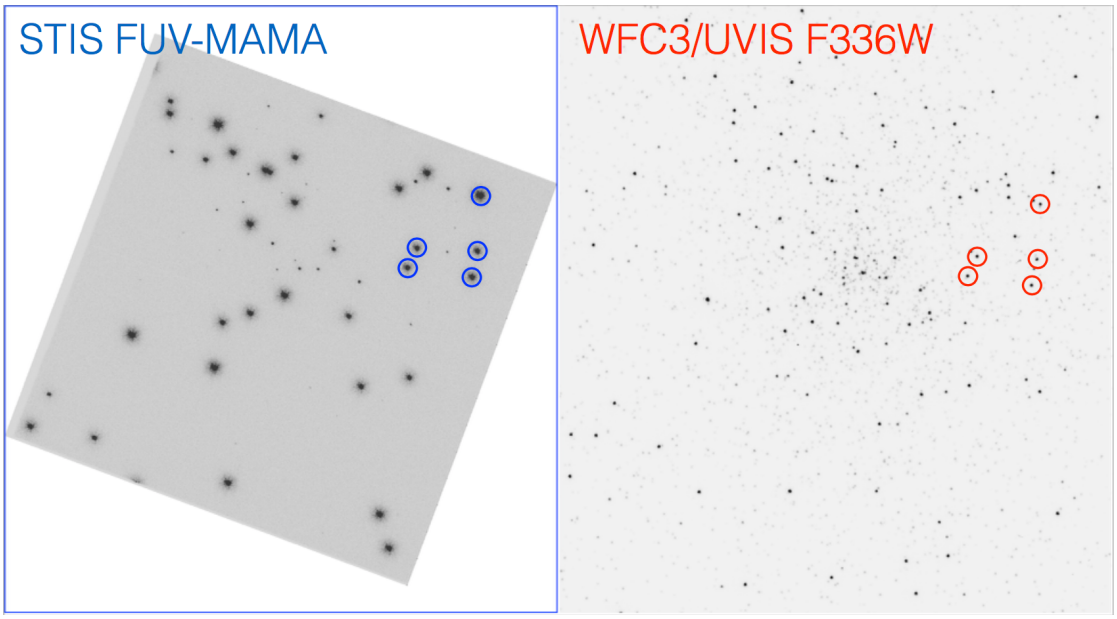

Figure 1.: Comparison of an example NGC 6681 calibration field in STIS FUV-MAMA (left) and WFC3/UVIS F336W (right). The FUV-MAMA image has been scaled and rotated to show the same field coverage as the WFC3/UVIS image. Five arbitrary stars used for the calibration are shown in both images (blue in left and red in right) to aid visual cross identification of globular cluster stars.

2.1 WFC3/UVIS Standard Astrometric Catalog

Table 1.: WFC3/UVIS F336W images used for creating the standard astrometric catalog.

Image	Date	Exp. Time	POS-TARG	PA_V3
`icau94v1q_flc.fits`	2013-09-05	294s	$(6.5, 6.5)$	272.0
`icau94v5q_flc.fits`	2013-09-05	294s	$(-6.5, -6.5)$	272.0
`icau95k9q_flc.fits`	2014-06-29	294s	$(6.5, 6.5)$	183.0
`icau95kdq_flc.fits`	2014-06-29	294s	$(-5.0, -0.0)$	183.0

To create the standard astrometric catalog, we used images of NGC 6681 obtained with the WFC3/UVIS as part of the HST UV Legacy Survey of Galactic Globular Clusters (Piotto et al. 2015). All NGC 6681 stars detected in the STIS FUV-MAMA are bright in the far-UV, but most of them are faint in the optical (> 4000 Å) bands. We have therefore chosen to use WFC3/UVIS images only obtained with the F275W and F336W filters. A summary of the WFC3/UVIS data sets used in this ISR can be found in Table 1. NGC 6681 was observed in two visits with the WFC3/UVIS. The telescope orientations for the two visits were separated by roughly 90°.

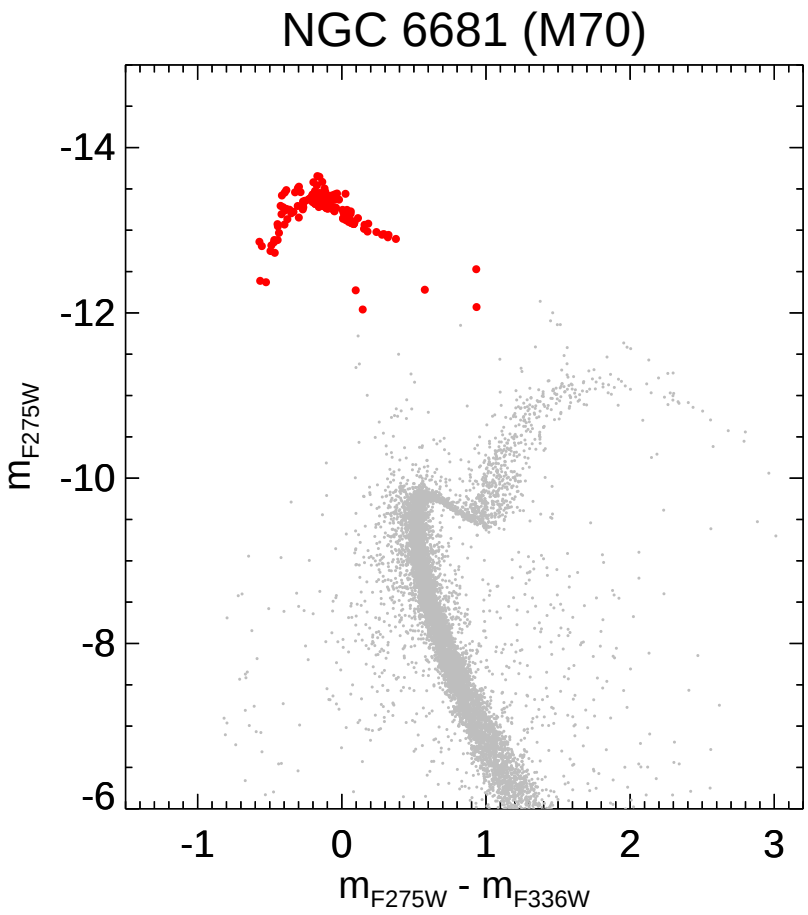

Figure 2.: Ultraviolet CMD of NGC 6681 using data obtained with WFC3/UVIS. Colors and magnitudes are given in $m_{\rm F275W} - m_{\rm F336W}$ and $m_{\rm F275W}$, respectively. Red dots show the stars selected as reference sources for the STIS FUV-MAMA, while gray dots are all other stars in the field.

We downloaded the `_flc.fits` files from the archive, and measured positions and fluxes of NGC 6681 stars by running the library-based PSF-fitting routine `img2xym_wfc3uv` program on individual F275W and F336W images. Stars that are detected in both F275W and F336W were matched in position to construct a color-magnitude diagram (CMD) as shown in Figure 2. From this, we selected UV-bright stars (i.e., stars with $m_{\rm F275W} - m_{\rm F336W} < 1$ and $m_{\rm F275W} < -12$ (m is defined as $-2.5\log_{10}[\rm counts]$), that mostly belong to the hot horizontal branch (HB) of NGC 6681. The selection of UV-bright stars was to ensure that the astrometric standard catalog only includes stars bright enough to have good positional measurements in the STIS FUV-MAMA images.

The `img2xym_wfc3uv` program outputs geometrically-corrected (x, y) positions based on the WFC3/UVIS distortion solutions by Bellini et al. (2011). These positions were used for registering the four individual WFC3/UVIS images in each

F275W and F336W band via a six-parameter linear transformation solution.[1] We then averaged the positions of stars and obtained rms scatter of positions. These positional rms of stars were compared against Fig. 5 of Bellini et al. (2011) to confirm that we are achieving the positional accuracy as expected from the WFC3/UVIS distortion solution.

2.2 STIS FUV-MAMA Catalog

Table 2.: STIS FUV-MAMA data used for deriving the geometric distortion solution.

Data sets	**DATE-OBS**
o40q02nkq, o40q02nmq, o40q02noq, o43n01nqq, o43n01nsq, o43n01nuq, o43n01nwq, o43n01nyq, o43n01o0q, o43n01o2q, o43n01o4q, o46h01csq, o46h01cyq	1997-09-29
o46h02tlq, o46h02tnq, o46h02tpq, o46h02trq	1998-03-29
o46h03kqq, o46h03kwq	1998-09-15
o46h04f9q, o46h04fbq, o46h04feq, o46h04ffq, o46h04fhq	1999-03-24
o49y01teq	1997-11-06
o5in01t9q, o5in01tfq, o5in01tlq	1999-09-17
o5in02czq, o5in02d1q, o5in02d3q, o5in02d9q, o69g01bdq, o69g01bjq, o69g01bpq	2000-09-18
o69g02h8q, o69g02hbq, o69g02hgq, o6i101onq, o6i101otq, o6i101ozq	2001-09-27
o6i102gkq, o6i102gmq, o6i102gsq	2002-02-26
o8h901w0q, o8h901w5q, o8h901w7q, o8h901w9q, o8h901wfq	2003-03-27
o8vw01efq, o8vw01ehq, o8vw01ejq, o8vw01eoq, o8vw01f4q	2004-03-04
obav01w4q, obav01w6q, obav01w8q, obav01waq, obav01wtq	2010-05-07
obmi01y4q, obmi01y6q, obmi01y8q, obmi01yaq, obmi01yiq	2011-04-16
obup01sgq, obup01siq, obup01skq, obup01smq, obup01sxq	2012-03-14
oc5301hrq, oc5301htq, oc5301hvq, oc5301i4q	2013-04-13
ocff01snq, ocff01spq, ocff01t3q, ocff01t5q, ocff01tpq	2014-04-10
ocrk01zhq, ocrk01zjq, ocrk01zlq	2015-04-10
od1q01naq, od1q01ncq, od1q01nfq, od1q01nhq, od1q01noq	2016-03-27
odbea1fmq, odbea1foq, odbea1fqq	2017-06-09

For the STIS FUV-MAMA data, we used images obtained with a clear aperture (25MAMA) to derive the geometric distortion solutions. Our original plan was to derive

[1]This solves for the offset, rotation, and scaling.

separate solutions for the MIRCUV (APERTURE = 25MAMA) and MIRFUV (APERTURE = F25QTZ or F25SRF2) optical elements, but we later found that our new distortion solution derived using MIRCUV data works well on images obtained with F25QTZ and F25SRF2 within the uncertainties of the solution (see Section 4.2 for details). We therefore decided to only derive a solution using MIRCUV data.

In total, we used 89 MIRCUV images as listed in Table 2. We downloaded the flat-fielded `_flt.fits` images from MAST archive and measured the position and brightness of stars using the `aper` photometry procedure in IDL – this uses the marginal Gaussian fitting method for determining positions of stars. Source crowding is not a concern for any of our FUV-MAMA image (see Figure 1 for an example), so a PSF-based measurement was unnecessary. Besides, we found that the quality of PSFs varies from one image to another, making the positional measurements unreliable.

3. Calibration

3.1 Analysis Steps

Our procedure for deriving the distortion solutions generally followed the method described in Kozhurina-Platais, V., et al. (2009), but with some significant deviations. Below, we provide details on each step involved in the derivation process.

(1) We first cross-matched stars in the standard astrometric catalog with those detected in the FUV-MAMA images. To do this, we transform the catalog positions to detector positions for each individual FUV-MAMA image listed in Table 2 using a 4-parameter linear solution that allows offsets (in each axis), rotation, and scaling. This linear solution is expressed in the following mathematical form:

$$\begin{aligned} x' &= \quad Ax + By + x_0 \\ y' &= -Bx + Ay + y_0 \end{aligned} \tag{1}$$

where (x, y) are the input positions and (x', y') are the output positions in the FUV-MAMA pixel coordinates. We start with an initial guess and iteratively solve for (A, B, x_0, y_0) with rejecting outliers until convergence is reached. This resulted in 20–40 matched stars per FUV-MAMA image, which provided reliable transformations.

(2) Once the matching process was completed for each image, we created lists of observed positions $(x_{\rm obs}, y_{\rm obs})$ and residuals $(\delta x, \delta y)$ of each star, where $\delta x = x_{\rm true} - x_{\rm obs}$ and $\delta y = y_{\rm true} - y_{\rm obs}$. The $(x_{\rm true}, y_{\rm true})$ positions are the catalog positions transformed to the FUV-MAMA pixel coordinates, and serve as the 'true' positions (i.e., where the stars *should* be detected if there were no geometric distortion) for the stars detected in the FUV-MAMA. We combined the lists of stars for all 89 FUV-MAMA images. Because the NGC 6681 images were taken in various telescope orientations (by observational design) and pointings (mostly due to

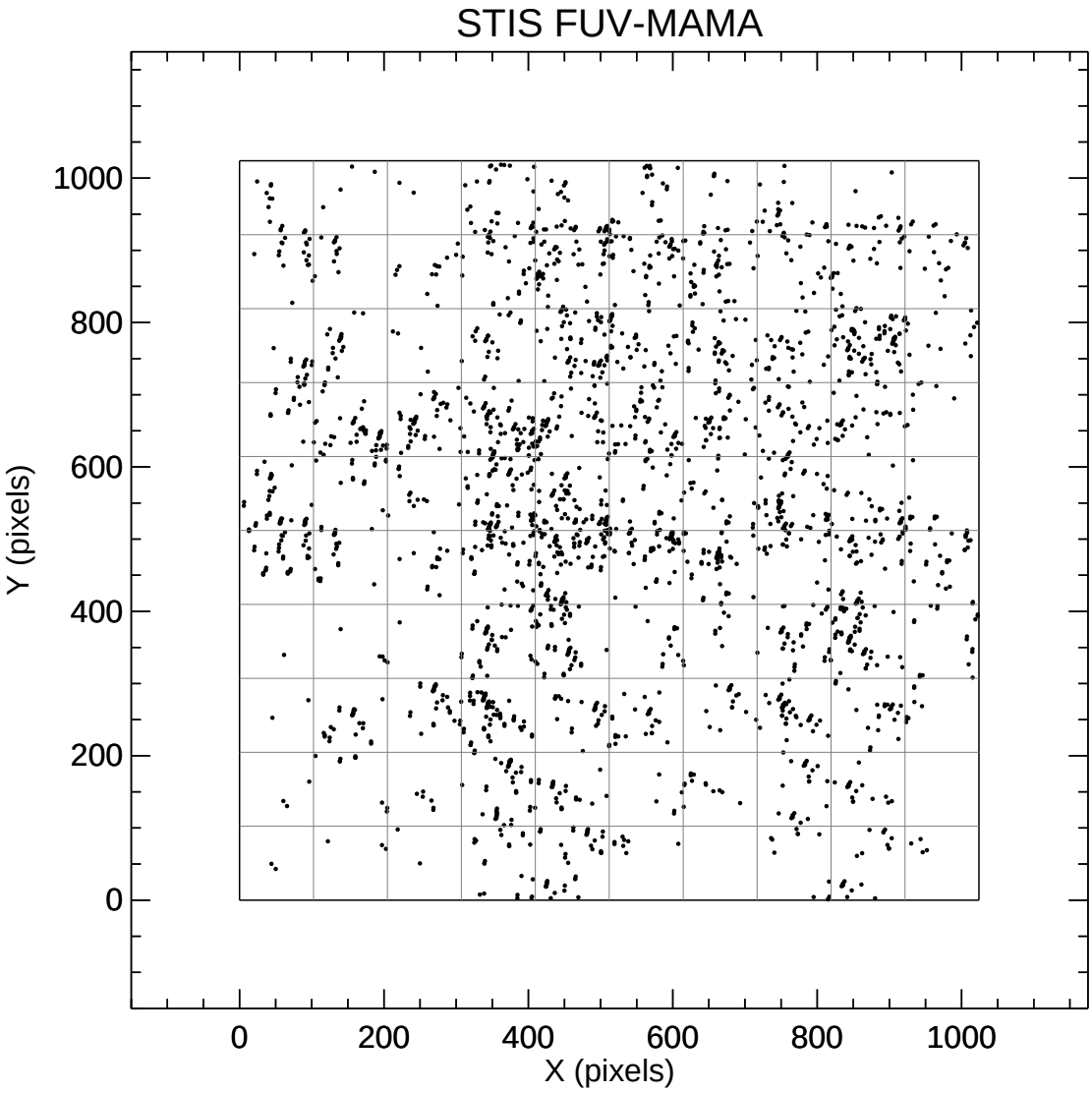

Figure 3.: STIS FUV-MAMA detector positions of NGC 6681 stars cross-matched with the WFC3/UVIS standard astrometric catalog. In total, there are 2,791 detections plotted as black dots. The regular horizontal and vertical lines show the 10×10 grid we adopted for deriving the geometric distortion solution.

the positional uncertainties in the guides stars used by HST), the globular cluster stars detected by the STIS FUV-MAMA cover a wide range in detector (x, y) coordinates. Consequently, we had calibration sources that cover the full field of view with enough sources per quadrant for reliable calibration. This is illustrated in Figure 3 where we plot the FUV-MAMA detector-based (x, y) position of all NGC 6681 stars matched with the astrometric standard catalog.

(3) We divided the detector coordinates into a 10×10 grid (see Figure 3) and for each

grid point, we calculated the average positions and residuals that represent the distortion correction required in each part of the detector. The distortion corrected position for each grid point is then simply represented as

$$\begin{aligned} x_{\rm corr} &= \bar{x}_{\rm obs} + \Delta x \\ y_{\rm corr} &= \bar{y}_{\rm obs} + \Delta y \end{aligned} \tag{2}$$

where Δx and Δy are the average of δx and δy in step (2). Following the standard distortion correction model used in the `IDCTAB` (Hack & Cox 2000, 2001), we represent the forward geometric distortion solution (i.e., observed $\rightarrow$ true positions) as the following fourth-order polynomial:

$$\begin{aligned} x_{\rm corr} &= c_{x,0,0} + \\ &\quad c_{x,1,0}\tilde{y} + c_{x,1,1}\tilde{x} + \\ &\quad c_{x,2,0}\tilde{y}^2 + c_{x,2,1}\tilde{x}\tilde{y} + c_{x,2,2}\tilde{x}^2 + \\ &\quad c_{x,3,0}\tilde{y}^3 + c_{x,3,1}\tilde{x}\tilde{y}^2 + c_{x,3,2}\tilde{x}^2\tilde{y} + c_{x,3,3}\tilde{x}^3 + \\ &\quad c_{x,4,0}\tilde{y}^4 + c_{x,4,1}\tilde{x}\tilde{y}^3 + c_{x,4,2}\tilde{x}^2\tilde{y}^2 + c_{x,4,3}\tilde{x}^3\tilde{y} + c_{x,4,4}\tilde{x}^4 \\ y_{\rm corr} &= c_{y,0,0} + \\ &\quad c_{y,1,0}\tilde{y} + c_{y,1,1}\tilde{x} + \\ &\quad c_{y,2,0}\tilde{y}^2 + c_{y,2,1}\tilde{x}\tilde{y} + c_{y,2,2}\tilde{x}^2 + \\ &\quad c_{y,3,0}\tilde{y}^3 + c_{y,3,1}\tilde{x}\tilde{y}^2 + c_{y,3,2}\tilde{x}^2\tilde{y} + c_{y,3,3}\tilde{x}^3 + \\ &\quad c_{y,4,0}\tilde{y}^4 + c_{y,4,1}\tilde{x}\tilde{y}^3 + c_{y,4,2}\tilde{x}^2\tilde{y}^2 + c_{y,4,3}\tilde{x}^3\tilde{y} + c_{y,4,4}\tilde{x}^4 \end{aligned} \tag{3}$$

where $\tilde{x} = (x_{\rm obs} - 512)$ and $\tilde{y} = (y_{\rm obs} - 512)$. The equation above allows one to calculate the distortion-corrected coordinates $(x_{\rm corr}, y_{\rm corr})$ given observed coordinates $(x_{\rm obs}, y_{\rm obs})$. A reverse distortion solution (true $\rightarrow$ observed positions) with coefficients $d_{x,i,j}$ and $d_{y,i,j}$ is similarly defined as in Equation 3, but the input coordinates now become $\tilde{x} = (x_{\rm corr} - 512)$ and $\tilde{y} = (y_{\rm corr} - 512)$. To keep the reference points of the detector coordinates for both the forward and reverse geometrical distortion corrections at the center of the detector, we adopt the following convention: $c_{x,0,0} = c_{y,0,0} = 0$ and $d_{x,0,0} = d_{y,0,0} = 0$. Then, we solved the geometric distortion polynomials (Equation 3) with the 10×10 grid of data points created above as inputs using a least-squares minimization algorithm.

Steps (1)–(3) above were iterated until the polynomial coefficients converged. To ensure that the iterations are improving the distortion solutions, we checked that for each iteration, the residuals decrease and provide better distortion-corrected positions. As evident in Figure 3, some grid points near the corners have significantly fewer number (or even none) of detections. These grid points were given lower weights (or ignored) when performing the solutions.

Table 3.: Polynomial coefficients for the FUV-MAMA geometric distortion solution.

i	j	$c_{x,i,j}$	$c_{y,i,j}$	$d_{x,i,j}$	$d_{y,i,j}$
0	0	0.000000000e+00	0.000000000e+00	0.000000000e+00	0.000000000e+00
1	0	−2.346813458e−05	2.451026177e−02	3.941604991e−02	4.079953922e+01
1	1	2.427007264e−02	−4.484187512e−05	4.120318897e+01	7.566731810e−02
2	0	1.584981859e−08	−5.427108105e−08	−2.654085222e−05	8.976903745e−05
2	1	1.238586312e−07	5.584123466e−09	−2.096121269e−04	−9.810409597e−06
2	2	−5.686955680e−09	1.845072272e−07	9.021989978e−06	−3.120811849e−04
3	0	9.821534833e−12	−4.343839277e−11	−1.573933579e−08	7.249155876e−08
3	1	−1.120214702e−10	2.636735916e−11	1.905659014e−07	−4.487949918e−08
3	2	3.464251745e−11	−1.567986544e−12	−5.790950452e−08	−3.269580294e−09
3	3	3.020217823e−11	1.396986362e−11	−5.278508075e−08	−2.539832738e−08
4	0	1.819768264e−13	−7.639717075e−14	−3.033630601e−10	1.255758928e−10
4	1	2.268814640e−13	1.277725915e−13	−3.843576148e−10	−2.124474122e−10
4	2	7.586840087e−14	1.167041365e−13	−1.289479662e−10	−1.929473768e−10
4	3	6.678498410e−14	−9.002936012e−14	−1.116286133e−10	1.559312599e−10
4	4	1.685402081e−14	−9.190396791e−13	−2.771746316e−11	1.569903230e−09

3.2 Results

The polynomial coefficients for the final solution are provided in Table 3, both for the forward ($c_{x,i,j}$ and $c_{y,i,j}$) and the reverse ($d_{x,i,j}$ and $d_{y,i,j}$) distortion corrections. The resulting distortion map is shown in Figure 4, where we illustrate the directions and relative magnitudes of the distortion corrections.

In Figure 5, we plot the residuals (observed−true positions) of the calibration sources when our geometric distortion solution is applied. For comparison, we also show the residuals without any correction – these are the original δx and δy used in the initial step (1) above. The rms of δx and δy for the gray dots in Figure 5 are 1.10 and 1.16 pixels, respectively, equivalent to 27.2 and 28.7 mas. With the geometric distortion solution applied (red dots), these become 0.16 pix or 4.0 mas in each coordinate. This represents the precision of our geometric distortion solution.

4. Implementation and Tests

4.1 STIS Pipeline and IDCTAB

Images obtained with the STIS FUV-MAMA detector are geometrically corrected as part of the **calstis** pipeline in the `GEOCORR` step (see STIS Data Handbook for details). The format of the `IDCTAB`, the reference file required in this step, is fully described in Hack & Cox (2001). For consistency with older versions of `IDCTAB` as well as other STIS reference files, the same mean pixel scales (the `SCALE` paramter) as in the previous `IDCTAB` (`o8g1508eo_idc.fits`) were used. The new `IDCTAB` with pa-

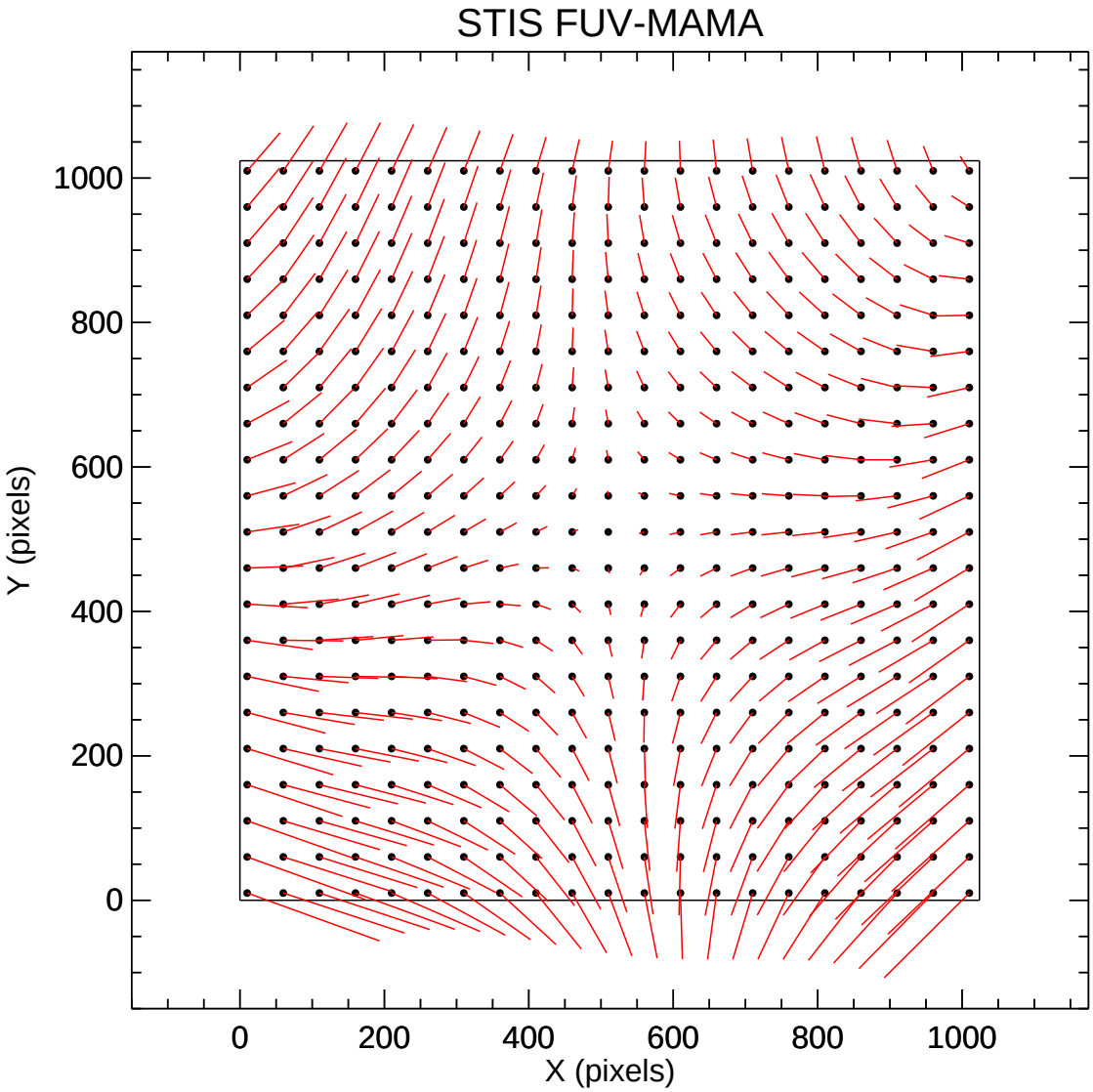

Figure 4.: Distortion map of the STIS FUV-MAMA. Black dots indicate the original positions, and red lines illustrate the direction and relative magnitude of the distortion corrections. Red lines are magnified by a factor of 30 for visualization. The longest red line corresponds to ~ 4 pixels in length.

rameters as listed in Table 3 is named `1771408ro_idc.fits`, and was implemented in the pipeline on July 7, 2017. Users that wish to manually apply the geometric distortion corrections for STIS FUV-MAMA images are advised to follow the steps below. For this example, the flat-fielded image is named `o1234567q_flt.fits`.

- Download the `IDCTAB` file from the following link:
  `https://hst-crds.stsci.edu/browse/1771408ro_idc.fits`
- Change the header parameters for keyword `IDCTAB` of the `o1234567q_flt.fits`

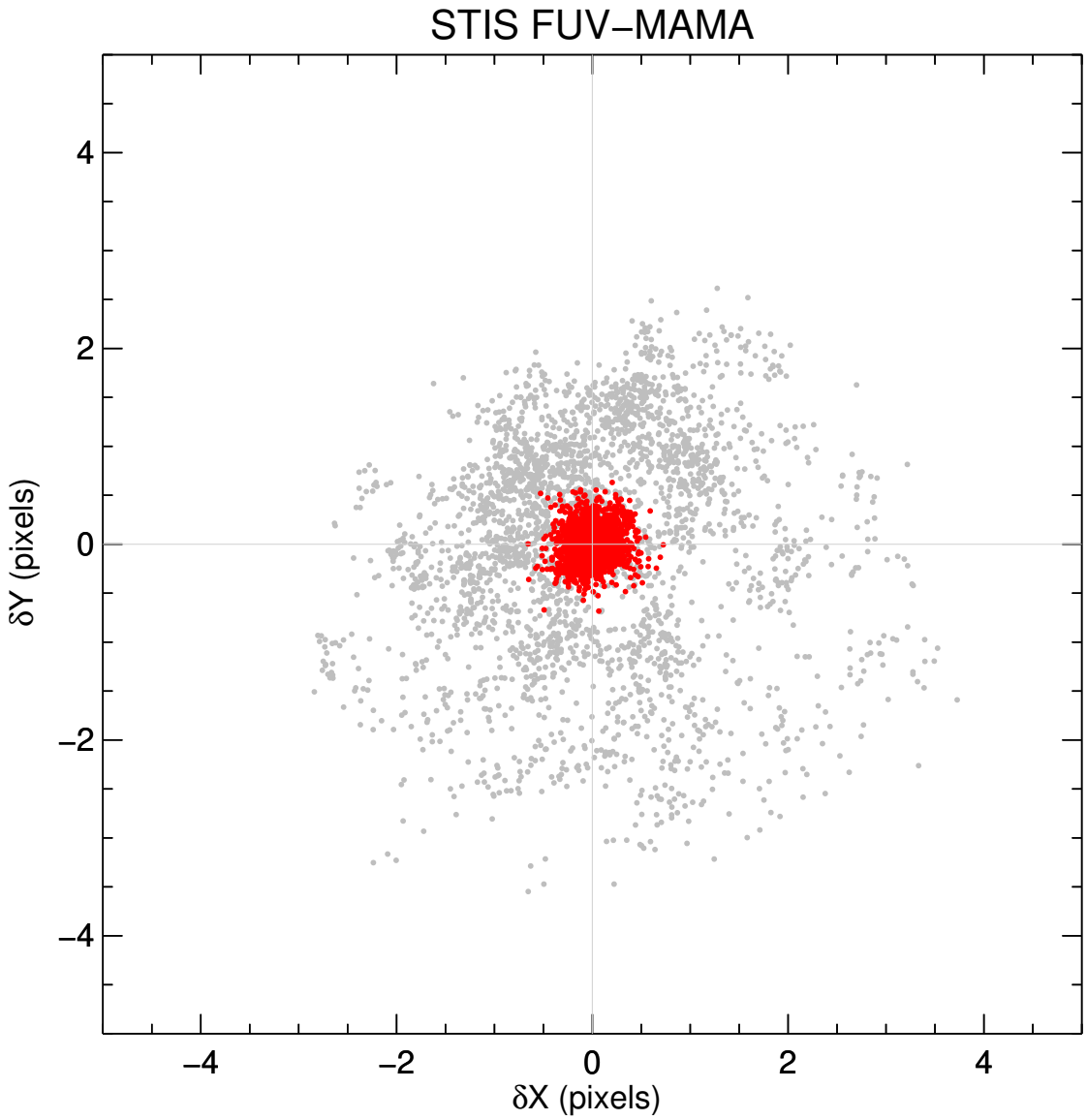

Figure 5.: Residual positions (i.e., observed−true) without the geometric distortion correction (gray dots), and with our new geometric distortion correction applied (red dots). Units are in STIS FUV-MAMA pixels. The average pixel scale for STIS FUV-MAMA is 0.0247 mas pix^{-1}.

image to this downloaded file. If the downloaded `IDCTAB` file is located in the same directory as the flat-fielded image, the header should look like:
`IDCTAB = './1771408ro_idc.fits'`

- Verify that the header keyword `GEOCOR` is set to `PERFORM`.
- Run `calstis` on the `o1234567q_flt.fits` image. This will create the geometrically-corrected image with the name `o1234567q_flt_x2d.fits`. In

AstroConda, running `calstis` will look like below:

```
>>> import stistools
>>> stistools.calstis.calstis('o1234567q_flt.fits')
```

4.2 Tests

We carried out a few tests with our newly derived geometric distortion solution as follows. We first selected a random sample of our calibration data sets and corrected for the geometric distortion solution as outlined in the previous section. We measured positions of NGC 6681 stars in both the `_flt.fits` (not corrected) and the `_x2d.fits` (corrected) images. The standard astrometric catalog were transformed to these images using the linear transformation solution of Equation 1. We then compared the transformed positions to the observed stars for assessments. Figure 6 shows the result of this process for one example data set (`o5in01tfq`). We find that the transformed positions are far better aligned with the geometrically-corrected images, indicating that the distortion solutions are making significant improvements.

We also performed tests on data obtained with the F25QTZ and F25SRF2 apertures. We downloaded NGC 6681 calibration images obtained in these configurations, and rectified these images using the new distortion solution. We then repeated the process described above to calculate the residuals (transformed−observed positions) for each detected star. Figure 7 shows the same 2-d residuals as shown in Figure 5, but for F25QTZ and F25SRF2 data sets. The rms of residuals is ~ 0.18 pix in each coordinate, comparable to that of MIRCUV data. We conclude that our geometric distortion solution derived using MIRCUV data improves both MIRCUV and MIRFUV data to a similar precision level.

Acknowledgements

The author would like to specially thank Andrea Bellini and Vera Kozhurina-Platais for their advice in various stages of this work.

Change History for STIS ISR 2018-XX

Version 1: Monday 16th April, 2018- Original Document

References

Bellini, A., Anderson, J., & Bedin, L. R., 2011, PASP, 123, 622
Hack, W., & Cox, C., 2000, ACS ISR 2000-11
Hack, W., & Cox, C., 2001, ACS ISR 2001-008
Kozhurina-Platais, V., et al., 2009a, WFC3 ISR 2009-33
Kozhurina-Platais, V., et al., 2009b, WFC3 ISR 2009-34

Kozhurina-Platais, V., et al., 2015, ACS ISR 15-06
Malumuth, E., 1997, STIS FUV-MAMA Geometric Distortion.
STIS Post Launch Quick Look Analysis Report No. 41. STIS IDT, Greenbelt.
Piotto, G., Milone, A. P., Bedin, L. R., et al. 2015, AJ, 149, 91
Walsh, J. R., Goudfrooij, P., & Malumuth, E. STIS ISR 2001-02

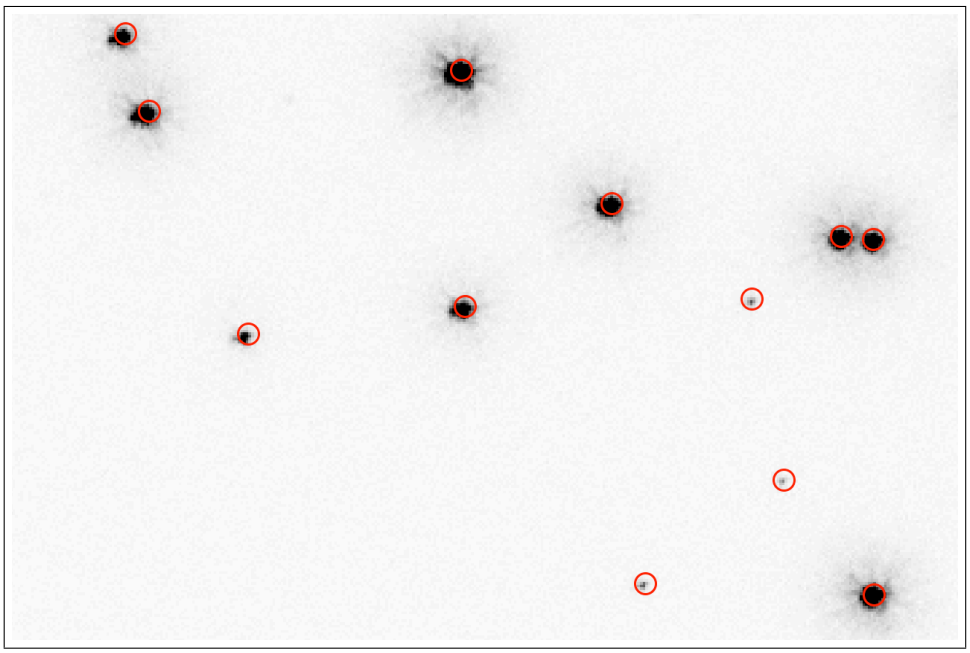

(a) Without geometric distortion correction.

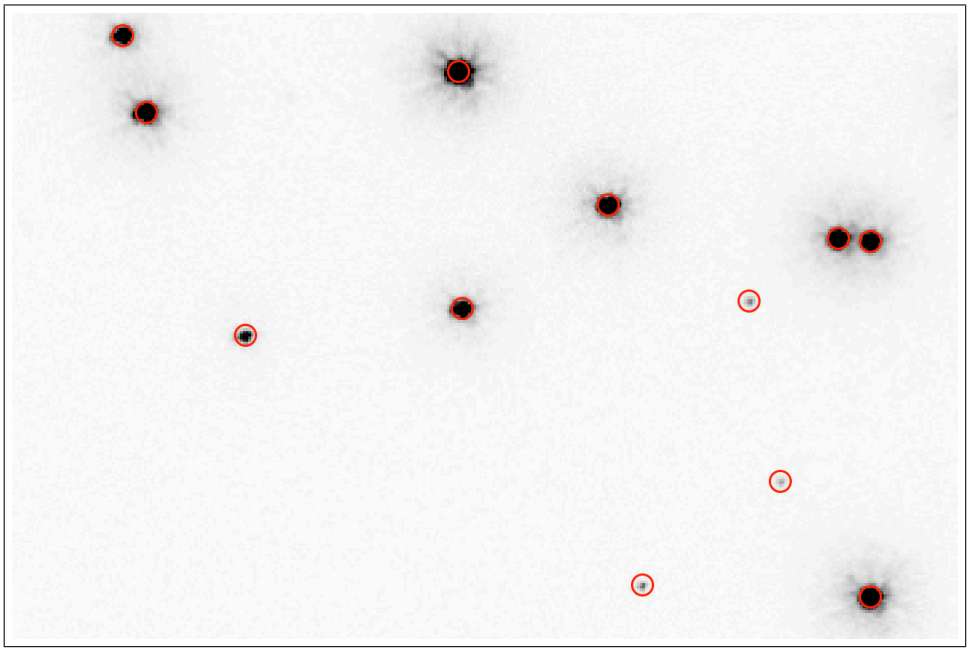

(b) With geometric distortion correction.

Figure 6.: Portion of the NGC 6681 field with stars circled in red. The top image shows the non-corrected `o5in01tfq_flt.fits`, and the bottom image shows the geometrically-corrected `o5in01tfq_flt_x2d.fits`. The red circles correspond to the standard astrometric catalog positions transformed to the individual images. Each image has a size of 350×230 pixel^2.

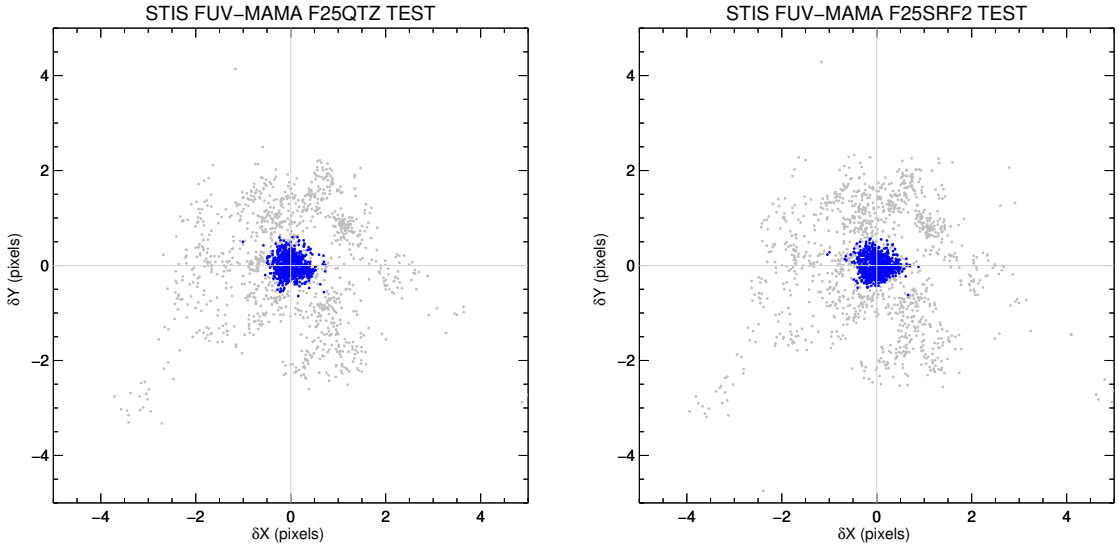

(a) Test on F25QTZ data sets.

(b) Test on F25SRF2 data sets.

Figure 7.: Same as in Figure 5, but for F25QTZ (left) and F25SRF2 (right) data sets. The residuals after correction are plotted in blue (instead of red).